Mutant MYO1F alters the mitochondrial network and induces tumor proliferation in thyroid cancer

Chiara Diquigiovanni[1], Christian Bergamini[2], Cecilia Evangelisti[3], Federica Isidori[1], Andrea Vettori[4], Natascia Tiso[4], Francesco Argenton[4], Anna Costanzini[1,2], Luisa Iommarini[2], Hima Anbunathan[5], Uberto Pagotto[1], Andrea Repaci[6], Giulia Babbi[2], Rita Casadio[2], Giorgio Lenaz[3], Kerry J. Rhoden[1], Anna Maria Porcelli[2], Romana Fato[2], Anne Bowcock[5], Marco Seri[1], Giovanni Romeo[1] and Elena Bonora [ID][1]

[1] Department of Medical and Surgical Sciences, DIMEC, St. Orsola-Malpighi Hospital, University of Bologna, Bologna, Italy
[2] Department of Pharmacy and Biotechnology, FABIT, University of Bologna, Bologna, Italy
[3] Department of Biomedical and Neuromotor Sciences, DIBINEM, University of Bologna, Bologna, Italy
[4] Department of Biology, University of Padova, Padova, Italy
[5] National Heart and Lung Institute, Imperial College, London, United Kingdom
[6] Endocrinology Unit, St. Orsola-Malpighi Hospital, Bologna, Italy

Familial aggregation is a significant risk factor for the development of thyroid cancer and familial non-medullary thyroid cancer (FNMTC) accounts for 5–7% of all NMTC. Whole exome sequencing analysis in the family affected by FNMTC with oncocytic features where our group previously identified a predisposing locus on chromosome 19p13.2, revealed a novel heterozygous mutation (c.400G > A, NM_012335; p.Gly134Ser) in exon 5 of *MYO1F*, mapping to the linkage locus. In the thyroid FRTL-5 cell model stably expressing the mutant MYO1F p.Gly134Ser protein, we observed an altered mitochondrial network, with increased mitochondrial mass and a significant increase in both intracellular and extracellular reactive oxygen species, compared to cells expressing the wild-type (wt) protein or carrying the empty vector. The mutation conferred a significant advantage in colony formation, invasion and anchorage-independent growth. These data were corroborated by *in vivo* studies in zebrafish, since we demonstrated that the mutant MYO1F p.Gly134Ser, when overexpressed, can induce proliferation in whole vertebrate embryos, compared to the wt one. *MYO1F* screening in additional 192 FNMTC families identified another variant in exon 7, which leads to exon skipping, and is predicted to alter the ATP-binding domain in MYO1F. Our study identified for the first time a role for *MYO1F* in NMTC.

Cancer Genetics and Epigenetics

Introduction

Familial aggregation is a significant risk factor for the development of thyroid cancer derived from follicular epithelial cells (non-medullary thyroid carcinoma, NMTC). When the primary cancer site is considered, the thyroid gland shows the highest estimate of familial relative risk among all organs (5- to 10-fold compared to 1.8 and 2.7 for breast and colon cancer, respectively).[1] Familial NMTC (FNMTC) accounts for 5–7% of all NMTC and may occur as a part of familial cancer syndromes (familial adenomatous polyposis, Gardner's syndrome, Cowden's disease, Carney's complex type 1, Werner's syndrome and papillary renal neoplasia) or as a primary feature (familial NMTC) (for a review see Ref. 2,3). FNMTC has become a well-recognized, unique clinical entity. Although still debated, there are some epidemiologic and clinical kindred studies that have shown an association between FNMTC and more aggressive behavior than sporadic cases, with higher rates of multicentric tumors, lymph node metastasis and extrathyroidal invasion, a younger age of onset and shorter disease-free survival.[2–4] A search for

What's new?

Evidence suggests that familial non-medullary thyroid carcinoma (FNMTC) is highly heterogeneous, complicating the identification of underlying mutations in family pedigrees. Here, investigation of chromosome 19p13.2, which contains a known thyroid cancer-predisposing locus, led to the identification of a novel mutation in the gene *MYO1F*. Relative to wild-type controls, thyroid cell models carrying mutant *MYO1F* exhibited a significant increase in colony formation and greater potential for invasion and anchorage-independent growth. Mutated cells further showed an altered mitochondrial phenotype, similar to the one observed in human thyroid tumors. The findings suggest that *MYO1F* has a role in thyroid cancer predisposition.

susceptibility genes, undertaken using linkage-based approaches, led to the identification of several predisposing loci: MNG1 (14q32), TCO (19p13.2), fPTC/PRN (1q21), NMTC1 (2q21), FTEN (8p23.1-p22) and the telomere–telomerase complex.[2,3] Mutations were identified at the 14q31 locus in the *DICER1* gene, which encodes for an enzyme required for miRNA maturation.[5] Recent data have also shown that dysregulation of miRNA expression is a hallmark of thyroid cancer[6] and an altered splicing regulation has been reported in FNMTC patients carrying a germline mutation in the *SRRM2* gene, encoding a splicing machinery subunit.[7] Additional studies have identified predisposing risk-variants in non-coding genes, including miRNAs[8] and a long non-coding gene *PTCSC2*.[9] Mutations in genes encoding regulators of the RAS pathway such as *RASAL1*[10] and *SRGAP1*[11] were also identified in FNMTC cases. Taken together, these data indicate that the genetic predisposition to FNMTC is characterized by a high degree of heterogeneity, hampering the identification of the underlying mutations in the corresponding pedigrees.

We previously mapped a predisposing locus for FNMTC on chromosome 19p13.2 in a multigenerational family with multiple individuals affected by thyroid carcinoma with oncocytic features (oxyphilia; TCO), with autosomal dominant inheritance.[12] In our study, we report whole exome sequencing (WES) data and functional studies providing evidence that mutant *MYO1F*, mapping to the TCO locus on chromosome 19p13.2, lead to NMTC.

Materials and Methods

The study was approved by the committee for protection of persons in biomedical research of Lyon (CCPRB A-96.18) and by the IARC Ethical Review Board (Project 95–050, amendment 01–013). Informed consents were obtained by clinicians, in each collaborating center.

Subjects

The TCO family has been previously reported[12] and the main clinical characteristics are reported in the Supporting Information. Papillary thyroid carcinomas (PTCs) were diagnosed in individuals II-5, III-3 and III-7 at the ages of 41, 27 and 11 years, respectively. In total, 192 FNMTC patients included in the mutation screening came from the families collected between 1996 and 2012 through the International Consortium for the Genetics of Non-Medullary Thyroid

Carcinoma; 149 female patients and 43 males were included (age of onset: 11–84 years, mean age = 42 years), thyroid cancer diagnosis is reported in Supporting Information Table S1.

WES analysis

WES was performed on three individuals from the TCO family, two affected by thyroid carcinoma with oncocytic features (individuals II-3; III-7, Fig. 1*a*) and one affected by adenoma (II-4), according to the pipeline reported in the Supporting Information. Variants were confirmed by polymerase chain reaction (PCR) and direct sequencing.

Cell lines

The FRTL-5 cell line is a stable thyroid cell line derived from normal thyroid glands from 5 to 6-week-old Fisher rats.[13] All cells were cultured in 6H5 medium consisting of Coon's modified Ham's F12 medium (Sigma-Aldrich, St. Louis, MO) supplemented with 5% newborn calf serum (NCS) (Sigma-Aldrich), 1 μg/ml insulin, 10 nM hydrocortisone, 5 μg/ml apo-transferrin, 10 ng/ml gly-his-lys, 10 ng/ml somatostatin, 1 mU/ml TSH (Sigma-Aldrich, St. Louis, MO) and penicillin/streptomycin (EuroClone, Milan, Italy). Cells were propagated in a fully humidified atmosphere of 5% CO_2 at 37°C.

COS7 cells derived from monkey kidney tissue were grown in Dulbecco's modified Eagle's medium, 10% fetal bovine serum, 2 mM L-glutamine, 100 U/ ml penicillin and 100 μg/ml streptomycin, in a humidified incubator at 37°C with 5% CO_2.

pCMV6-MYO1F p.Gly134Ser plasmid generation *via* site-directed mutagenesis

The construct pCMV6 encoding wild-type (wt) *MYO1F* (RC207069) was purchased from OriGene OriGene Technologies, Rockville, MD) in frame with the tag (polypeptide chain containing the aminoacid sequence Asp-Tyr-Lys-Asp-Asp-Asp-Asp-Lys, or DYKDDDDK (DDK) and containing neomycin resistance (G418) for stable selection. The mutation c.400G > A was inserted using the Q5 Site-direct Mutagenesis kit, according to the manufacturer's instruction (New England Biolabs, Ipswich, MA) using the oligonucleotides forward 5′-AGGTGTCTGGCGGAAGCGAGAAGGTCCAG-3′ and reverse 5′-TGGAGATGTAGCCCATGATTATTTGGCT-3′. The site-directed mutagenesis was verified by plasmid direct sequencing.
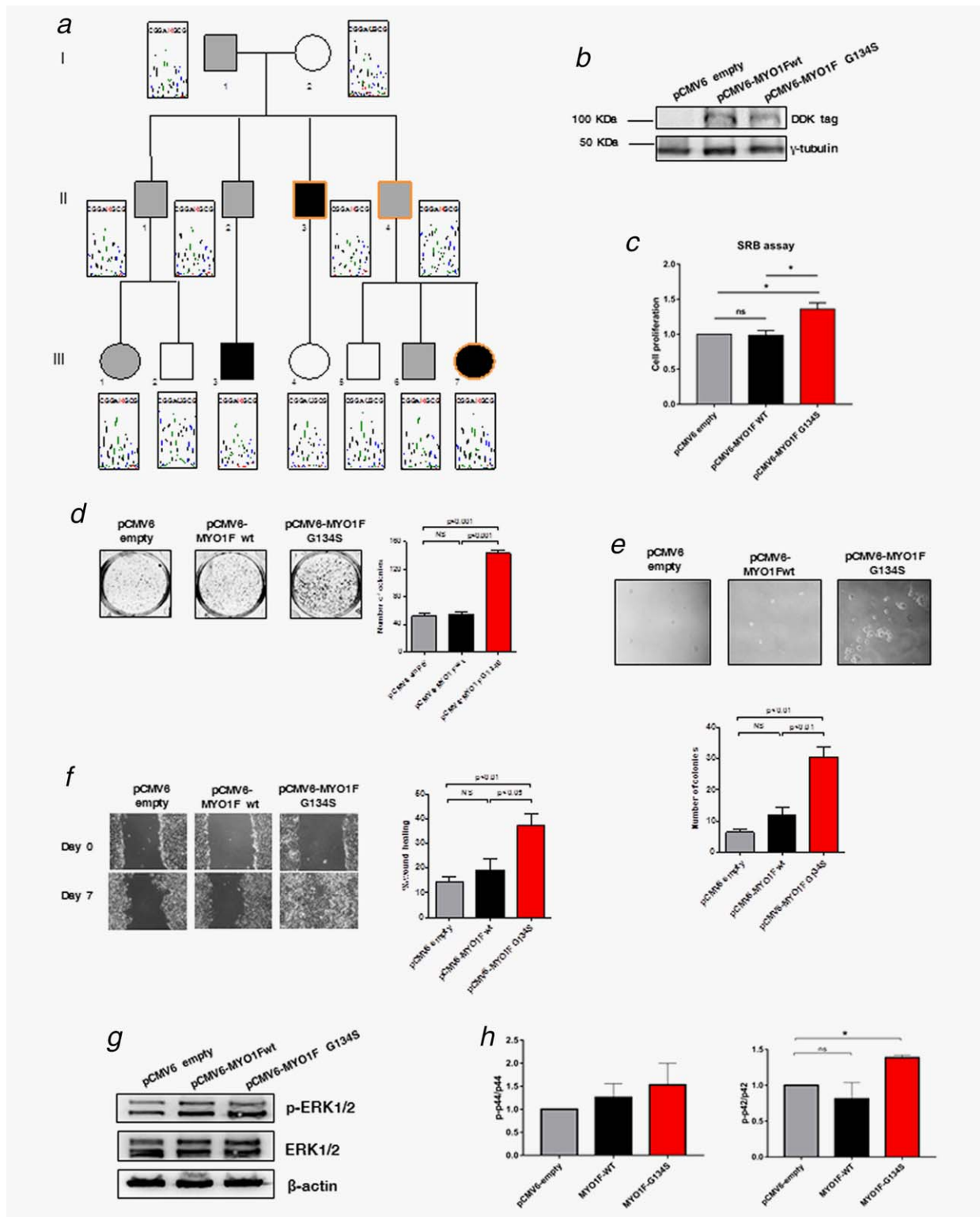
Figure 1. Study of MYO1F p.Gly134Ser variant. (*a*) Pedigree of the TCO family: electropherograms of the sequences of available family members, showing the co-segregation of the change (in red) with the oncocytic carcinoma (black)/adenoma (grey) phenotype. (*b–h*) Functional analysis of the MYO1F p.Gly134Ser variant. All experiments were repeated at least three times. Scale bars indicate standard error, stars indicate $p < 0.05$. (*b*) Western blot analysis showing the recombinant MYO1F protein in stably expressing FRTL-5 cells, using a specific anti-DDK antibody. Cell stably transfected with the empty vector are indicated as pCMV6-empty. Cells stably expressing the wt protein are indicated as pCMV6-MYOF wt, cells stably expressing the mutant protein are indicated as pCMV6-MYOF G134S. (*c*) SRB assay showed a significant increase in cell growth and proliferation for the pCMV6-MYOF G134S cells. (*d*) Plate colony formation potential using SRB assay showing an increased number of colonies formed by FRTL-5 expressing the mutant MYO1F protein, compared to cells expressing either the empty vector or the wt protein. (*e*) Growth in soft agar: FRTL-5 cells expressing the MYO1F mutant protein p.Gly134Ser significantly generated more colonies, compared to the empty and the cells expressing the wt protein. (*f*) Wound healing assay: FRTL-5 cells expressing the MYO1F mutant protein p.Gly134Ser filled the gap significantly faster compare to the other two cell lines. (*g, h*) Western blotting analysis of ERK1/2 phosphorylation in the three cell lines and densitometric quantification. [Color figure can be viewed at wileyonlinelibrary.com]

Generation of FRTL-5-stably transfected cell lines

A 7.5-μg of pCMV6 empty, pCMV6-MYO1F-wt and pCMV6-MYO1F-G134S plasmids were transfected using liposomes according to the manufacturer's instructions (Lipofectamine 2000, ThermoFisher Scientific, Grand Island, NY). Forty eight hours after transfection, selection was obtained by supplementing complete medium with 500 μg/ml G418 (ThermoFisher Scientific) for 2 weeks. Isolated clones were grown with 200 μg/ml G418.

Western blot

A detailed protocol is reported in the Supporting Information, including the list of primary antibodies used.

Sulforhodamine B (SRB) assay to investigate cell proliferation and plate colony formation

For cell growth and proliferation assays, 2.5×10^5 cells were seeded in duplicate and incubated 96 hours at 37°C. For plate colony formation, 2.5×10^4 cells were seeded in duplicate and incubated for 20 days at 37°C. Cells were washed in phosphate-buffered saline (PBS) and fixed with cold trichloroacetic acid (TCA) 50% at 4°C for 1 hr, then TCA was eliminated and cells were dried at room temperature for 16 hrs. Cells were stained with SRB 0.4% in 1% acetic acid for 30 min, washed with 1% acetic acid for four times. For the proliferation assay, cells were solubilized in TrisHCl 10 mM pH 10.5, mixing for 10 min on a rotatory plate. Absorbance was read at $\lambda = 564$ nm using a Beckman Coulter DU-530 spectrophotometer. For plate colony assay, cells were photographed with ChemiDoc XRS+ (Biorad). Area and number of colonies were quantified with the *ImageJ* software (National Institute of Health, Bethesda, MD) discarding colonies <1 pixel.

Soft agar colony assay

Stable cell lines were seeded in triplicate in a 0.48% top agar in growth medium over a layer of 0.8% agar in a six-well plate at a density of 1×10^5 cells/ml. Plates were incubated at 37°C and 5% CO_2 for 12 days, monitoring for colony formation. Medium was replaced every 5 days. After 12 days, colonies were photographed and analyzed with *ImageJ* software.

Wound healing assay

Stable cell lines were plated onto six-well plates and allowed to form a confluent monolayer. The cell monolayer was then scratched in a straight line to make a "scratch wound" with a 10-μl tip and the cell debris was removed by washing the cells with PBS. 5H5 (6H5 medium without Thyroid-Stimulating Hormone (TSH)) medium supplemented with 10% NCS and 200 μg/ml of neomycin was added with or without 1 mM *N*-acetyl-L-cysteine (NAC), and images of the closure of the scratch were captured at 0 and 7 days. Images were analyzed with the *TScratch* software.[14]

Iodide transport

Iodide uptake by FRTL-5 cells was measured by live cell imaging with the fluorescent halide biosensor yellow fluorescent protein (YFP)-H148Q/I15L, as described previously.[15,16]

Mitochondrial morphology and mass assessment *via* live cell imaging

Mitochondrial morphology was assessed by live imaging with or without 1 mM NAC, using a Nikon Eclipse 80 microscope (Nikon, Tokio, Japan) according to Ref. 17. Circularity measurements were collected using *ImageJ* standard tools.

Mitochondrial mass measurements

In 96-well culture plates, 1×10^4 FRTL-5-stable cell lines were seeded in quadruplicates. The next day, cells were loaded with 50 nM MitoTracker Green (MTG) for 30 min at 37°C in complete medium. After washing twice with medium, MTG fluorescence was recorded in a plate reader (EnSpire, PerkinElmer). MTG fluorescence values were expressed as relative fluorescence unit (RFU)/viable cells. Cell viability was assessed with a resazurin-based method.

Mitochondrial potential measurement *via* JC-1

The fluorescent probe JC-1 (5, 5′,6, 6′-tetrachloro-1, 1′, 3, 3′-tetraethylbenzimidazol carbocyanine iodide) was used to measure the mitochondrial membrane potential ($\Delta\phi$), as described in the Supporting Information.

Cellular respiration

Oxygen consumption in intact cells. Approximately 1.5×10^6 FRL5-stable cell lines were harvested at 70–80% confluence, washed in PBS, resuspended in complete medium and assayed for oxygen consumption at 30°C using a thermostatically controlled oxygraph chamber (Instech Mod. 203, Plymouth Meeting, PA). Basal respiration was measured in their respective media and compared with the one obtained after injection of oligomycin (1 μM) and Carbonyl cyanide-p-trifluoromethoxyphenylhydrazone (FCCP) (1–6 μM). Antimycin A (5 μM) was added at the end of experiments to completely block the mitochondrial respiration. Data were normalized to protein content determined by the Lowry method.

ATP/ADP synthesis ratio determination. Nucleotides were extracted and detected using a Kinetex C18 column (250 × 4.6 mm, 100 Å, 5 μm; Phenomenex, CA), with a two pump Agilent 1100 series system. Absorbance (260 nm) was monitored with a photodiode array detector (Agilent 1100 series system). Nucleotide peaks were identified by comparison and coelution with standards and quantification by peak area measurement compared with standard curves.[18]

ROS quantification

Intracellular ROS. FRTL-5-stable cell lines were seeded at 5×10^4 cells per well and incubated 16 hrs. Cells were treated with 10 μM 2',7'-dichlorodihydrofluorescein diacetate

(DCFDA) dissolved in medium for 1 hr. Then, cells were washed twice with PBS and incubated for 12 hrs in complete medium. Finally, cells were washed with PBS and the fluorescence emission from each well was measured ($\lambda exc = 485$ nm; $\lambda em = 535$ nm) with a multi-plate reader (Enspire, Perkin Elmer). Data are reported as the mean $\pm$ SD of at least three independent experiments.

Extracellular ROS. FRTL-5-stable cell lines were seeded at 5×10^4 cells per well and incubated 16 hrs. Cells were treated with 10 μM Amplex red (N-acetyl-3,7-dihydroxyphenoxazine), 0.025 U/ml horseradish peroxidase dissolved in complete medium for 16 hrs. The medium was collected and measured (λexc 530, λem 590) with a multiplate reader (Enspire, Perkin Elmer). Data were normalized for cell number using resazuring assay. Data are reported as the mean $\pm$ SD of at least three independent experiments.

In vivo study of mutant MYO1F

Zebrafish embryos and adults were maintained and mated according to standard procedures. Mutant and wt capped *MYO1F* mRNAs were synthesized with the SP6 mMESSAGE mMACHINE kit (Ambion, ThermoFisher Scientific) using as template the PCS2 + MYO1F-G134S and PCS2 + MYO1F-wt plasmids, respectively. wt zebrafish embryos were injected at one-cell stage with 150 pg of MYO1F-wt or MYO1F-G134S mRNA and then fixed at 48 hrs post fertilizations (hpf). To determine the cell proliferation patterns, a whole-mount immunostaining with the anti-phospho-Histone H3 (pH3) antibody (Millipore, Darmstadt, Germany) was performed. We counted the mitotic cells along the trunk of each fish (from the yolk extension to the tip of the tail) and calculated the average number of pH3-positive cells per embryo to compare the difference among groups. Statistical analysis was performed using Student's unpaired *t* test. Differences were considered significant for $p < 0.05$.

MYO1F mutation screening in FNMTC pedigrees

PCR primers for human *MYO1F* (NM_012335) were designed with Primer3 v4.0 (http://primer3.ut.ee) and are available on request. Genomic DNA extracted from peripheral blood was amplified according to standard PCR conditions, and PCR products were analyzed by direct sequencing, as reported in the Supporting Information.

P1 pAltermax MYO1F exon 7-minigene generation

PCR of *MYO1F* genomic region encompassing exons 7 and 8 was performed using primer forward 5′ GGGGAATT-CAGAAGGGAAGAGAGGCAAGG-3′, inserting an *EcoRI* restriction site, and primer reverse 5′-CCCTCTAGAAAC-TCAGGAGGGTTTCTGGG-3′, inserting an *XbaI* restriction site from a heterozygous carrier. We generated the minigene reporter as described previously.[19] The PCR products were cloned into the digested P1 pAltermax and plasmids sequenced to identify the plasmids with the wt or the

variant alleles. The splicing alteration analysis was performed as reported in Ref. 19 and in Supporting Information.

Structural modeling

Modeling of the protein structure was performed adopting a building obtained by comparison procedures based on MODELLER (https://salilab.org/modeller/). The template was MYO1C_HUMAN (PDB code: 4BYF_A), and the final structural superimposition indicated a 45% sequence identity among the computed and experimental structures. Given the coverage of the template to the target, modeling was possible in the protein region spanning amino acids 16–714. From structural superimposition, it was also possible to locate the ATP-binding domain.

Statistical analysis

Statistical analyses were performed using the one-way analysis of variance (ANOVA) with Tukey's multiple comparison test. All tests were completed using Prism (GraphPad, San Diego, CA). A $p < 0.05$ was considered statistically significant. All experiments were carried out at least in triplicates.

Results

Identification of a novel missense mutation in MYO1F conferring tumor-like properties to thyroid cells

WES was performed in three members of the original TCO family where the linkage locus was identified[12] (II-3, II-4 and III-7; Fig. 1a), in two individuals affected by thyroid carcinoma and one affected by thyroid adenoma, all with oncocytic features. All variants were queried with ANNOVAR and filtered based on Single Nucleotide Polymorphisms Database (dbSNP) database annotation. Potentially deleterious mutations were selected according to their functional class, and prioritization was given to those lying in the chr19p13.2 linkage region and present in all three cases. A unique novel heterozygous variant in the linkage interval shared by all three individuals fulfilled the criteria for pathogenicity: the mutation c.400G > A in *MYO1F* cDNA (NM_012335), leading to a missense p.Gly134Ser substitution, predicted to be damaging by PolyPhen-2 and Provean (Supporting Information Table S2), not present in the NHLBI Exome Sequencing Project (ESP), in the Exome Aggregation (ExAc) and Genome Aggregation (gnomAD) databases and absent from 1000 in-house control chromosomes. The variant co-segregated with the carcinoma/adenoma phenotype in the family and appeared to be a likely candidate for the NMTC gene residing at 19p13.2 (Fig. 1a). *MYO1F* consists of 28 exons encoding a 1098-amino-acid protein of the class of unconventional myosins.[20] The p.Gly134Ser amino acid change resides in a very well conserved position in the ATP-binding domain of the protein. Since thyroid tumor tissue from patients was not available for additional studies, we generated cell models stably expressing the wt or mutant MYO1F (mut) after transfection with the corresponding
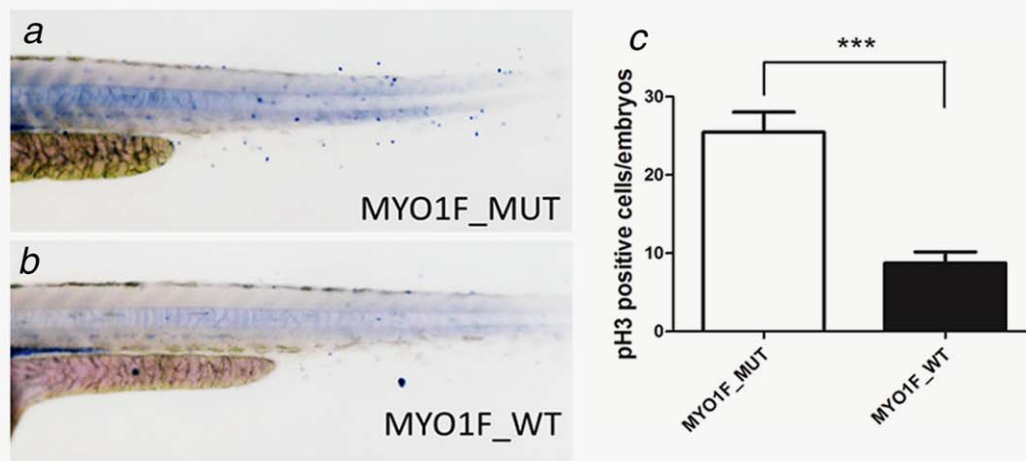
Figure 2. Proliferation analysis in zebrafish overexpressing either wt or mutant MYO1F p.Gly134Ser: (*a,b*) Immunostaining of phospho-histone H3 (pH3) performed in 48 hpf zebrafish larvae. An increase in cell proliferation can be observed in embryos injected with mutant MYO1F mRNA compared with embryos injected with the wt transcript of MYO1F. (*c*) Quantification of pH3-positive cells in injected embryos (48 hpf) was performed with manual counting of mitotic cells (blue nuclei) along the left side of the embryonic trunk, between the yolk extension and the tip of the tail. For each group, 22 embryos were analyzed (MYO1F_MUT: 25.45 ± 2.584; MYO1F_WT: 8.727 ± 1.445). ***, $p < 0.001$, Student's unpaired *t* test. [Color figure can be viewed at wileyonlinelibrary.com]

episomal plasmids, and a control cell line stably expressing the corresponding empty vector, pCMV6, *via* G418 selection. We used highly differentiated and functional FRTL-5 rat thyroid cell line[13] to reveal the effects of the MYO1F variant. The p.Gly134Ser mutation was inserted by site-directed mutagenesis in the construct encoding wt *MYO1F* in frame with the DDK tag. Western blotting with anti-DDK antibody in stably transfected cells showed that both wt and mut proteins were expressed in similar amounts (Fig. 1*b*). Stable cell lines expressing either the wt or the mut MYO1F protein were tested for their proliferative and tumorigenic potential in comparison with cells transfected with the empty vector. A significant increase in the proliferation was observed in mut cells, compared to cells expressing either the empty vector or the wt recombinant protein (one-way ANOVA with Tukey's multiple comparisons test $p = 0.0044$; pCMV6 empty *vs.* pCMV6-MYO1F G134S, $p = 0.0092$; pCMV6-MYO1F WT *vs.* pCMV6-MYO1F G134S $p = 0.0072$; pCMV6 empty *vs.* pCMV6-MYO1F WT $p = 0.9853$, Fig. 1*c*). A significant increase in the number of colonies in anchorage-dependent and independent growth was also observed in mut cells, compared to cells expressing either the empty vector or the wt recombinant protein (one-way ANOVA $p < 0.0001$, Fig. 1*d*). Anchorage-independent growth was monitored as colony formation in soft agar. Mutant MYO1F-expressing cells showed a significant increase in colony formation in soft agar, compared to cells stably transfected with the wt protein or the empty vector (ordinary one-way ANOVA $p = 0.0005$; Fig. 1*d*, lower panel).

The wound-healing assay, showed that mutant cells had a significantly greater invasive potential after 7 days in culture, compared to cells stably transfected with the empty vector or the wt protein, as quantified with *TScratch* software[14]

(ordinary one-way ANOVA $p = 0.0024$; Fig. 1*e*). The wound healing assay was performed in a medium lacking TSH. Since proliferation of thyroid cells is totally TSH-dependent, we could discriminate between proliferation and invasiveness. Therefore, our data do indeed indicate that the mutant cells have a greater invasive potential.

To relate the observed changes in growth to the activation of specific cellular pathways, we investigated different kinases with key roles in cell proliferation and migration, including Akt and ERK1/2. We found a specific increase in the phosphorylation of ERK1/2 kinases in cells expressing the mutant protein, in particular for the p42 isoforms (Figs. 1*f* and [1]*g*; $p = 0.0042$, empty *vs.* pCMV6 MYO1F G134S). Taken together, these findings support a role for the MYO1F mutation in the modulation of tumorigenic potential *in vitro* (*i.e.*, in the modulation of proliferation and invasivity).

Mutant MYO1F p.Gly134Ser stimulates proliferation in zebrafish embryos

To analyze the pro-proliferative function of MYO1F *in vivo*, we evaluated the effects of the human p.Gly134Ser MYO1F protein in zebrafish (*Danio rerio*) embryos. The zebrafish genome encodes a single *myo1f* orthologue (GenBank ref seq. NM_001256671.2; NP_001243600.1), with 85% similarity and 76% identity at amino acidic level to human MYO1F. Notably, the position corresponding to human Glycine 134 is conserved in the zebrafish Myo1f protein, indicating a putative functional role of this aminoacidic residue (Supporting Information Fig. S1).

To test whether the mutant MYO1F variant can induce cell proliferation *in vivo*, one-cell stage embryos were injected with either wt or p.Gly134Ser MYO1F mutated mRNA. At 48 hpf, the injected embryos were fixed and stained with antibodies

Cancer Genetics and Epigenetics

against phospho-histone H3 (pH3), a widely used marker to reveal cell mitosis in zebrafish.[21–23] Embryos injected with the mutant mRNA showed a significant increase in the number of pH3-positive cells, compared to their siblings injected with the MYO1F wt allele (Figs. 2a and 2b). In particular, we observed an increased number of mitotic cells, especially in the caudal region ($p < 0.0001$, Fig. 2c) indicating that, when ubiquitously expressed, the MYO1F mutant protein can induce proliferation also in zebrafish embryos.

Iodide influx is not altered by the mutation MYO1F p.Gly134Ser

FRTL-5 cells are highly differentiated thyroid cells and a suitable model to measure iodide transport in vitro. We measured iodide uptake by live cell imaging after transient transfection with a vector encoding YFP-H148Q/I152L, a modified YFP whose fluorescence is quenched by I^- in a concentration-dependent manner.[15,16] We did not detect any differences in I^- uptake between the different cell lines (one-way ANOVA $p = 0.4816$; Supporting Information Figs. S2a and S2b).

Mutation MYO1F p.Gly134Ser alters the mitochondrial network

Since the oncocytic phenotype is characterized by mitochondrial hyperplasia in the tumors of affected individuals of the TCO family,[12] we analyzed the mitochondrial network of stably transfected FRTL-5 cells by live-cell microscopy using the Mito-Tracker Green probe. Mitochondria in the mutant cell lines appeared more fragmented compared to mitochondria in wt and empty cell lines (Fig. 3a), as shown by the significant increase in circularity value of mutant cells mitochondria when compared to wt and empty cell mitochondria (Fig. 3b).

The total mitochondrial mass was significantly greater in mutant cell lines, as determined by MitoTracker fluorescence quantification, normalized for cell viability using a resazurin-based assay (ordinary one-way ANOVA $p < 0.0001$; Fig. 3c). The increase in mitochondrial mass in the mutant cells was confirmed via Western blotting for voltage-dependent anion-selective channel (VDAC) (ordinary one-way ANOVA $p = 0.0136$, Fig. 3d).

Since an impaired mitochondrial network may alter mitochondrial function, we evaluated the levels of proteins and their phosphorylated forms (phospho-DRP1), involved in mitochondrial fission/fusion, that is, DRP1 and MFN1, but we did not detect any significant difference between the various cell lines (Figs. 3e and [3]f; Supporting Information Figs. S3a and S3b, respectively).

We measured the mitochondrial membrane potential and oxidative phosphorylation (OXPHOS) activity of the different cell lines. The mitochondrial membrane potential was measured with the probe JC-1,[24,25] and normalized for cell viability using a resazurin-based assay. No differences were found between empty vector-expressing cells, wt and mutant cells (one-way ANOVA $p = 0.0720$; Supporting Information Fig. S3c). The addition of oligomycin A did not alter the

fluorescence ratio of JC-1, indicating that ATP hydrolysis by ATPase was not involved in maintaining the mitochondrial potential (Supporting Information Fig. S3c).

We measured the ATP/ADP ratio in the different cell lines, showing that the cells expressing mutant MYO1F exhibit a significant lower ratio in comparison to wt cells, due to the concomitant decrease in ATP and increase in ADP levels ($p = 0.0289$, one-way ANOVA, Fig. 3g). However, there were no differences in respiratory activity between the different cell lines under basal conditions (one-way ANOVA $p = 0.5014$, Supporting Information Fig. S3d) in the ratio of FCCP/oligomycin-treated cells (one-way ANOVA $p = 0.3900$; Supporting Information Fig. S3e. Extracellular lactate measurement also showed no changes between the different cell lines (ordinary one-way ANOVA $p = 0.4069$; Supporting Information Fig. S3f).

ROS are elevated in FRTL-5 cells expressing MYO1F p.Gly134Ser

Since differentiated thyroid cells produce a great amount of hydrogen peroxide (H_2O_2) necessary for thyroid hormone synthesis,[26] we investigated whether reactive oxygen species (ROS) production in transfected FRTL-5 cell lines was deranged by the MYO1F mutation.

Intracellular ROS levels, measured with the fluorescent probe DCF-DA, were significantly increased in the mutant cells (one-way ANOVA $p = 0.0015$, Fig. 4a). To understand whether this phenomenon was due to alterations/decreases of intracellular ROS detoxifying enzymes, we performed Western blotting analysis of catalase, mitochondrial manganese superoxide dismutase (SOD2) and peredoxin-3 (Prx3), using GAPDH as endogenous reference. The steady state levels of the analyzed proteins were not significantly different between all cell lines (Fig. 4b; Supporting Information Figs. S4a–S4c; one-way ANOVA $p = 0.1328$ for catalase, $p = 0.8592$ for SOD2, $p = 0.6837$ for Prx3).

Interestingly, treatment for 24 hrs with the antioxidant compound NAC partially recovered the defects in the mitochondrial network in cells expressing mutant MYO1F, confirming the role of ROS in mitochondrial fragmentation ($p < 0.0001$; Fig. 4c). In concordance, we observed a decrease in cell invasion between the FRTL-5 cell lines treated with NAC, compared to the untreated ones, as measured by the wound healing assay (Student's t test, untreated vs. treated $p = 0.0236$ pCMV6 empty, $p = 0.0338$ pCMV6-MYO1F wt, $p = 0.0488$ pCMV6-MYO1F-G134S; Fig. 4d). This effect was observed in all cell lines, not only for the mutant MYO1F cells.

To measure extracellular ROS, we used the fluorescent probe Amplex Red, which is unable to cross the plasma membrane. We observed a significantly higher amount of extracellular ROS in mutant cell lines, compared to the empty vector-transfected cells and the wt ones. Moreover, we detected, a significant decrease in extracellular ROS in the cells expressing MYO1F wt, when compared to the empty vector (one-way ANOVA $p = 0.0004$; pCMV6-empty vs.
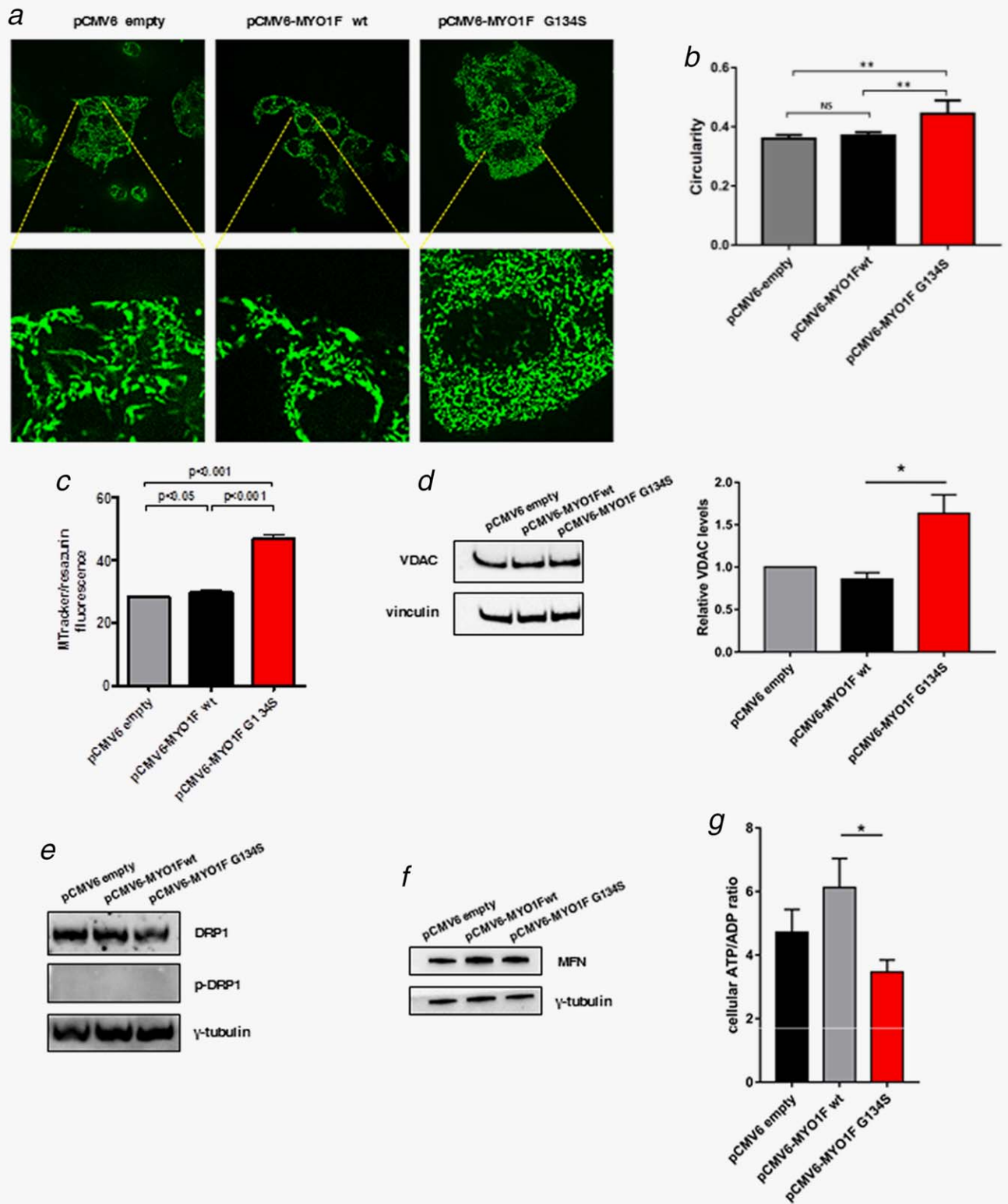
Figure 3. Mitochondrial defects in FRTL-5- MYO1F p.Gly134Ser cells. (*a*) Representative fluorescence images of pCMV6-empty, pCMV6-MYOF wt, and pCMV6-MYOF G134S stained with Mitotracker Green to evaluate mitochondrial network. The cells expressing the mutant protein show more circular (*b*) and more abundant (*c*) mitochondria and more fragmented mitochondrial network in comparison with wt and cells bearing empty vector. MitoTracker signal quantification was normalized on viable cell number assessed by resazurin-based assay. (*d*) Representative image of Western blotting analysis for VDAC in pCMV6-empty, pCMV6-MYOF wt, and pCMV6-MYOF G134S cells and relative quantification, compared to reference protein (vinculin). Scale bars indicate standard errors. Stars indicate significant *p* values. (*e*–*f*) Representative images of Western blotting analysis for DRP1-phospho-DRP1 (*e*) and MFN1 (*f*) in pCMV6-empty, pCMV6-MYOF wt, and pCMV6-MYOF G134S cells. (*g*) ATP/ADP ratio in cellular extracts from pCMV6-empty, pCMV6-MYOF wt, and pCMV6-MYOF G134S cells, showing a decreased ATP/ADP ratio in the mutant FTRL5 cells. Scale bars indicate standard errors. Stars indicate significant *p* values. [Color figure can be viewed at wileyonlinelibrary.com]
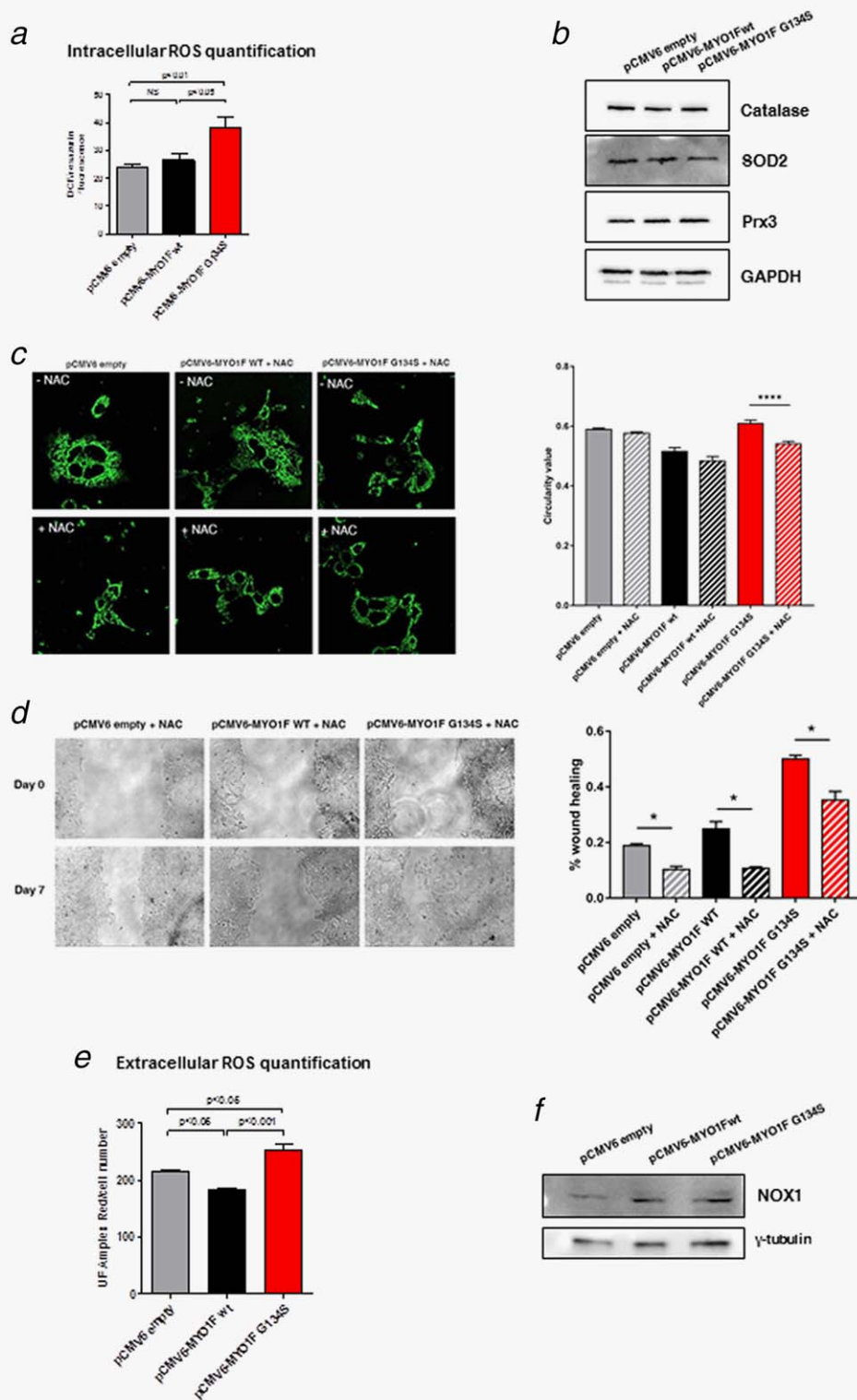
Figure 4. ROS production. (*a*) Intracellular ROS production measured by DCFDA fluorescent probe. Data show a significant ROS production increase in the FRTL-5 cells expressing MYO1F p.Gly134Ser in comparison to wt and cells bearing the empty pCMV6 vector. Data are expressed as arbitrary fluorescence units ± SD, normalized on viable cell number. (*b*) Representative Western blot analysis showing the expression of detoxifying enzymes (catalase, SOD2, and Prx3) in the three cell lines. GAPDH was used as endogenous loading control. (*c*) Representative fluorescence images of pCMV6-empty, pCMV6-MYOF wt, and pCMV6-MYOF G134-S cells stained for 24 hrs with 1 mM *N*-acetyl-L-cysteine (NAC) or vehicle. Live cells were stained with 40 nM Mitotracker Green to evaluate mitochondrial network. Circularity value analysis was performed using *ImageJ* software standard tool. Data indicate a significant recovery for the NAC-treated mutant cells *versus* the untreated mutant ones. (*d*) Wound healing assay in presence of NAC and relative quantification, showing a significant decrease in invasive potential in the cell lines. (*e*) Extracellular ROS production measured by Amplex red fluorescent probe. Data show that FRTL-5 cells expressing MYO1F p.Gly134Ser presented the highest levels of extracellular ROS, whereas the cells expressing the wt protein presented a reduced amount of extracellular ROS. Data are expressed as arbitrary fluorescence units ± SD normalized on viable cell number. Cell viability was assessed by resazurin-based method. (*f*) Representative image of Western blotting analysis for NOX1 in pCMV6-empty, pCMV6-MYOF wt, and pCMV6-MYOF G134S cells. [Color figure can be viewed at wileyonlinelibrary.com]

Table 1. Rare coding variants identified in *MYO1F*-targeted mutation screening

Chr19 genomic position (hg19)	Amino acid change (NP_036467)	MAF in famNMTC ($N = 192$)	MAF in gnomAD (European only)
g.8616995 C>T rs184748543	p.Lys186[1]	0.0026	0.004224
g.8615552C>T rs201962739	p.Pro266	0.0026	0.001478
g.8615513C>G	p.Gly368[2]	0.0026	0
g.8610599G>T	p.Ile430	0.0026	0
g.8587411C>T rs201982814	p.Val1024Met[3]	0.0026	0.0007455[4]

[1]SNV not changing the corresponding amino acid, but with an altered ESE profile compared to wt cDNA, and removing SR-binding domains. The SNV co-segregated with the NMTC phenotype in the available members of the corresponding family.
[2]SNV not segregating with the NMTC phenotype in the corresponding families.
[3]Missense variant predicted to be "benign" (PolyPhen-2) and "tolerated" (SIFT).
[4]One homozygous individual present in European population.

pCMV6-MYO1F wt $p < 0.05$; pCMV6-MYO1F wt *vs.* pCMV6-MYO1F G134S $p < 0.001$; Fig. 4*e*). We evaluated NOX1 protein levels, but we did not detect any significant variation between the different cell lines (Fig. 4*f*; Supporting Information Fig. S4*d*; one-way ANOVA $p = 0.5900$).

Mutation screening of human MYO1F in FNMTC patients

To identify additional patients carrying predisposing germline mutations in *MYO1F*, we performed a mutation screening *via* Sanger sequencing of genomic DNA from peripheral blood of 192 independent FNMTC cases. These patients represented a heterogeneous group of cases affected by PTC/FTC, and the presence of oncocytic features was not always investigated. These data were available only for a small subgroup of patients (Supporting Information Table S1). We identified several rare/novel coding variants in *MYO1F* (Table 1), including a rare silent change in exon 7, present in both the affected individuals of the corresponding family, from whom DNA was available (Supporting Information Fig. S5*a*). This change potentially removed an exonic sequence enhancer (ESE) in exon 7, as predicted by the ESE Finder v3.0 program (Supporting Information Fig. S5*b*). The change, corresponding to the genomic coordinates chr19:g.8616995C > T (rs184748543), was present with a minor allele frequency (MAF) of 0.003168 in the general population and a MAF of 0.004224 in individuals of European ancestry-only (gnomAD; Table 1). The variant frequency was not significantly different between the NMTC cases and general population controls; moreover, one individual in the gnomAD database was homozygous for the variant allele, suggesting that it might have no severe functional consequences.

Nevertheless, to study whether it could hamper the inclusion of exon 7 in the final *MYO1F* transcript, since no fresh RNA was available from the affected patients carrying the rs184748543 variant allele, we generated a minigene plasmid carrying either the wt or mutant sequence, and transfected simian COS7 cells to study transcription (Figs. 5*a* and 5*b*). RT-PCR with minigene-specific synthetic primers and direct sequencing revealed that the wt exon was correctly spliced, whereas the mutant transcript lacked exon 7 (Fig. 5*c*). This altered transcript is predicted to produce a shorter MYO1F protein, with an in-frame deletion of 43 amino acids (G169-Q212) in the motor domain of MYO1F, that may alter the structure of the ATP-binding domain in the molecular motor of MYO1F (residues 110–117 and 162–166; Fig. 5*d*).

Discussion

The etiology of differentiated thyroid cancer is still poorly understood, but this type of cancer is influenced by both genetic and environmental factors. Large genome-wide case–control association studies have identified genetic variants conferring NMTC susceptibility in the general population.[27–29] A number of common single nucleotide polymorphisms (SNPs) have been reported to be associated with NMTC risk, but few studies have been conducted in high-risk NMTC families to examine the transmission of the risk allele to the affected members.[30]

In our study, we report the identification of MYO1F as the gene mutated at the TCO locus. We provide functional evidence that the MYO1F p.Gly134Ser mutation leads to an increased oncogenic potential *in vitro*, in terms of cell growth and invasion. FRTL-5 cells, a cell model resembling a functional thyrocyte,[13] stably transfected with the plasmid encoding mutant MYO1F p.Gly134Ser showed increased proliferation, generated significantly more colonies in soft agar and showed a significantly greater invasive potential compared to cells stably transfected with the empty vector or with wt *MYO1F*.

These *in vitro* data were supported by *in vivo* findings in zebrafish, showing that the mutant MYO1F p.Gly134Ser, when overexpressed, can induce proliferation in whole vertebrate embryos, supporting the idea that the novel missense change identified in exon 5 of *MYO1F* is the causative mutation at the TCO locus.

The TCO locus in the original pedigree was associated with an oncocytic phenotype, that is, enriched in mitochondria.[12] Previous work by our group uncovered a tight correlation between the co-occurrence of mitochondrial DNA (mtDNA) alterations in oncocytic thyroid cancer, and a marked dysfunction of OXPHOS complexes, in particular complex I.[31–33] Since thyroid follicular cells generate H_2O_2 by membrane-bound dual oxidases for the synthesis of thyroid hormones, these cells are at increased risk of oxidative stress
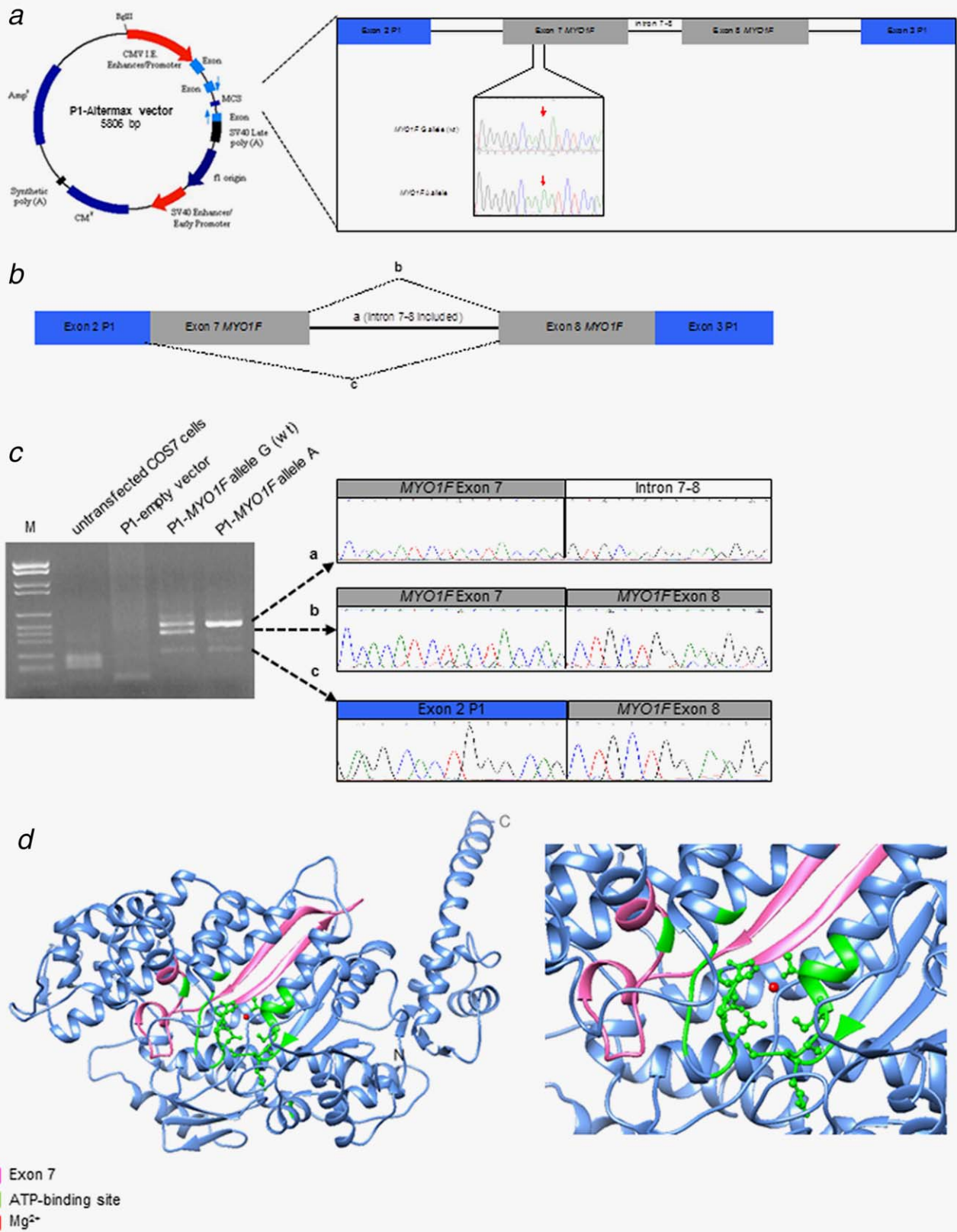
Figure 5. MYO1F rs184748543. (*a*) Map of the minigene plasmid, showing the genomic insert of the wt and mutant alleles (red arrows). (Blue arrows = position of the primers used for the specific RT-PCR). (*b*) RT-PCR of COS7-transfected with the *MYO1F* allele-specific mini-genes. *Upper panel*: predicted final transcripts generated by the correct splicing of mini-gene-specific exons (blue) and *MYO1F*-specific exons (grey). *Lower panel*: 2% agarose gel image (left) of the RT-PCR products, showing the different sizes of the transcripts and corresponding electropherograms (right): the wt *MYO1F* allele promoted the inclusion of the exon 7 in the final transcript, whereas the mutant allele induced an exon skipping in the final transcript, as predicted by the removal of the ESE in the exon 7. (*d*) Structure prediction of the MYO1F molecular motor region, with the ATP-binding region highlighted in green. Pink indicates the residues corresponding to exon 7 and red is the ion of magnesium. [Color figure can be viewed at wileyonlinelibrary.com]

and ROS-mediated DNA damage. Indeed, an imbalance between pro- and anti-oxidative factors has been suggested as an important mechanism in thyroid tumorigenesis.[34,35] Oxidative stress generated by mitochondrial dysfunction can also promote migration and stimulate MAPK-mediated cell death. We therefore sought to evaluate: (*i*) the functionality of the mitochondrial respiratory chain as a whole; (*ii*) the response to oxidative stress of FRTL-5 cells stably expressing the wt or mutant recombinant MYO1F protein, compared to cells expressing the empty-vector. We found that the mitochondrial membrane potential and OXPHOS activities were similar in all cell lines, suggesting that mitochondria were still functional. However, analysis of the mitochondrial network by live-cell visualization revealed that in the mutant cell lines, mitochondria appeared as separated rod-shaped organelles.

The mitochondrial features of mutant MYO1F cells were therefore reminiscent of the oncocytic features described previously in the tumor tissues of the patients carrying the p.Gly134Ser change.[12]

In our experimental setting, we found that cells with the MYO1F p.Gly134Ser mutation, in addition to having an altered mitochondrial network and an increased mitochondrial mass, produced significantly more intracellular and extracellular ROS.

It has been reported that the establishment and maintenance of a transformed state is related to the presence of extracellular ROS, in particular, superoxide anion generated by a specific membrane-associated NADPH-oxidase, NOX1.[35] In fact, oncogenic activation of proliferative/mitogenic pathways has been associated with increased ROS production due to activation of the membrane-bound NADPH oxidases.[36] We did not detect differences among NOX1 protein levels, but this finding did not exclude an increased activation of this enzyme in the cells carrying the mutant MYO1F protein. Extensive analysis of tumor cell lines derived from different tissues, including thyroid carcinomas, has shown that they were all characterized by extracellular ROS generation, not found in cells derived from normal tissues.[34] This is paralleled by our findings, since extracellular ROS production was increased only in FRTL-5 cells expressing the mutant MYO1F p.Gly134Ser protein, suggesting that the mutation is sufficient to generate a transformed phenotype.

Interestingly, when the cells with the MYO1F p.Gly134Ser mutation were treated with an antioxidant (NAC), we observed a partial but significant rescue of the mitochondrial fragmentation, confirming the role of ROS in this phenomenon.[37] In agreement with this result, treatment with NAC also decreased the invasiveness of all cell lines including mutant MYO1F cells, as indicated by the wound-healing assay. These pilot data on phenotype rescue suggest that the treatment with antioxidants may be effective for this type of tumors.

Since the "mitochondria-rich" phenotype may be underreported by histologic analysis,[32] we screened additional FNMTC patients to identify other *MYO1F* germline variants that could predispose to thyroid tumor development.

However, the available samples represented a heterogeneous group of familial cases affected by NMTC, and the high genetic heterogeneity of thyroid cancer might have hampered the discovery of a number of additional predisposing variants in *MYO1F*. We identified a rare variant in two affected sibs in exon 7, which promoted the skipping of the exon from mature mRNA *in vitro*. No data regarding the presence of an oncocytic phenotype were available for the two affected sibs. In addition, the unavailability of fresh RNA from tissues of these patients prevented us from confirming that this exon skipping event actually occurs *in vivo*. Moreover, the allele frequency of the exon 7 variant allele in our FNMTC cases was not significantly different from the one present in the control individuals in public databases; therefore, its contribution to NMTC predisposition remains elusive. Our results regarding MYO1F mutation screening in FNMTC cases stress once again the high genetic heterogeneity underlying familial thyroid cancer. Nevertheless, our study shows that a defective MYO1F protein promotes the development of an oncocytic phenotype, that is, mitochondrial proliferation, indicating that this cellular characteristic can develop not only from mitochondrial DNA defects[31–33] but also from nuclear defects in specific genes, that is, *MYO1F*. Mitochondrial dysfunction and stress has been widely related to cancer, in particular, in thyroid cancer predisposition.[31,32] More broadly, an altered mitochondrial function is a hallmark of many cancers, although the nature of functional modification depends on the type of cancer.[33]

It is interesting to note that F-actin is one of the few known interactors of MYO1F[20] and has been recently implicated in mitochondrial fission control.[38] Blockade of F-actin polymerization/depolymerization altered the mitochondrial network.[38] Similarly to what has been observed in other autosomal dominant disorders due to mutations in myosin genes, such as MYH9,[39,40] we can hypothesize that the modified conformation of MYO1F may block actin filament recycling; therefore, concurrently altering the mitochondrial network organization.

Recent data have shown the contribution of mitochondrial dynamics toward tumor initiation and progression, although the exact mechanism is not known. Excessive fission and reduced fusion is a feature of many tumors.[41–43] For example, in human pancreatic cancer, expression of oncogenic Ras/activation of MAPK pathway induces ERK2-mediated Drp1 phosphorylation leading to increased mitochondrial fragmentation and the inhibition of this phosphorylation in xenografts is sufficient to block tumor growth.[44] Interestingly, recent data indicated that ERK2 also phosphorylated MFN1 to control mitochondrial morphology and apoptosis.[45] We did not find difference in Drp1 levels and phosphorylation in our cell models, and it will be of interest to evaluate also this pathway in the framework of the observed altered mitochondrial network present in the mutant MYO1F cells.

It is becoming increasingly clear that mitochondrial fission and fusion play a critical role in quality control and mitochondrial damage/repair in cancer. Therefore, our data

Cancer Genetics and Epigenetics

showing a fragmented mitochondrial network due to MYO1F p.Gly134Ser mutation highlight a potential novel pathway that may be deranged in thyroid cancer, that is, an altered myosin/F-actin regulated interaction.[20]

To date, no other mutations have been reported in myosin-encoding genes in thyroid cancer; however, it is interesting that MYH9, a non-muscle myosin involved in sensorineural deafness and thrombocytopenia,[39,40] has recently been found to regulate the ncRNA genes PTCSC2 and FOXE1 at the 9q22 thyroid cancer susceptibility locus.[46] In the TCGA database, somatic mutations in MYO1F are reported in 352 cases from various cancer types (Supporting Information Fig. S6a). The mutation identified at the TCO locus in MYO1F was not reported. In the COSMIC database several mutations are present in MYO1F in different types of cancer (Supporting Information Fig. S6b), but only a somatic variant is reported in thyroid carcinoma (COSM4132813). However, MYO1F overexpression was reported in 24 of 513 (4.68%) cases (Supporting Information Fig. S6c). These and our data suggest that MYO1F dysregulation may predispose to cancer in a subgroup of cases. Indeed, the oncocytic phenotype, observed in the family with the MYO1F p.Gly134Ser mutation, represents a specific, although rare, group of thyroid neoplasms, in which MYO1F mutation screening may be more relevant than in other FNMTC cases. The identification of the molecular cause(s) of specific thyroid cancer subtypes will help tailor patients' treatment for a more personalized therapy.

URL

Catalogue of Somatic Mutations in Cancer (COSMIC): http://cancer.sanger.ac.uk/ ESEfinder 3.0: rulai.cshl.edu/tools/ESE/ Exome Aggregation database (ExAc): http://http://exac.broadinstitute.org/Genome Aggregation database (gnomAD): http://gnomad.broadinstitute.org/ MODELLER: https://salilab.org/modeller/ PolyPhen-2: genetics.bwh.harvard.edu/pph2 PROVEAN (including SIFT): provean.jcvi.org/ Primer 3: primer3.ut.ee The Cancer Genome Atlas (TCGA): https://tcga-data.nci.nih.gov/

Acknowledgements

References

1. Malchoff CD, Malchoff DM. Familial nonmedullary thyroid carcinoma. Cancer Control 2006;13:106–10.

2. Guilmette J, Nosè V. Hereditary and familial thyroid tumours. Histopathology 2018;72:70–81.

3. Navas-Carrillo D, Ríos A, Rodríguez JM, et al. Familial nonmedullary thyroid cancer: screening, clinical, molecular andgenetic findings. Biochim Biophys Acta 2014;1846:468–76.

4. Bonora E, Tallini G, Romeo G. Genetic predisposition to familial nonmedullary thyroid cancer: an update of molecular findings and state-of-the-art studies. J Oncol 2010;2010:1

5. Rio Frio T, Bahubeshi A, Kanellopoulou C, et al. DICER1 mutations in familial multinodular goiter with and without ovarian Sertoli-Leydig cell tumors. JAMA 2011;305:68–77.

6. Dettmer M, Perren A, Moch H, et al. Comprehensive microRNA expression profiling identifies novel markers in follicular variant of papillary thyroid carcinoma. Thyroid 2013;23:1383–9.

7. Tomsic J, He H, Akagi K, et al. A germline mutation in SRRM2, a splicing factor gene, is implicated in papillary thyroid carcinoma predisposition. Sci Rep 2015;5:10566

8. Swierniak M, Wojcicka A, Czetwertynska M, et al. In-depth characterization of the microRNA transcriptome in normal thyroid and papillary thyroid carcinoma. J Clin Endocrinol Metab 2013;98:E1401–9.

9. He H, Li W, Liyanarachchi S, et al. Genetic predisposition to papillary thyroid carcinoma: involvement of FOXE1, TSHR, and a novel lincRNA gene, PTCSC2. J Clin Endocrinol Metab 2015;100:E164–72.

10. Liu D, Yang C, Bojdani E, et al. Identification of RASAL1 as a major tumor suppressor gene in thyroid cancer. J Natl Cancer Inst 2013;105:1617–27.

11. He H, Bronisz A, Liyanarachchi S, et al. SRGAP1 is a candidate gene for papillary thyroid carcinoma susceptibility. J Clin Endocrinol Metab 2013;98:E973–80.

12. Canzian F, Amati P, Harach HR, et al. A gene predisposing to familial thyroid tumors with cell oxyphilia maps to chromosome 19p13.2. Am J Hum Genet 1998;63:1743–8.

13. Meli A, Perrella G, Curcio F, et al. In vitro cultured cells as probes for space radiation effects on biological systems. Mutat Res 1999;430:229–34.

14. Gebäck T, Schulz MM, Koumoutsakos, et al. TScratch: a novel and simple software tool for automated analysis of monolayer wound healing assays. Biotechniques 2009;46:265–74.

15. Rhoden KJ, Cianchetta S, Stivani V, et al. Cell-based imaging of sodium iodide symporter activity with the yellow fluorescent protein variant YFP-H148Q/I152L. Am J Physiol Cell Physiol 2007;292:C814–23.

16. Rhoden KJ, Cianchetta S, Duchi S, et al. Fluorescence quantitation of thyrocyte iodide accumulation with the yellow fluorescent protein variant YFP-H148Q/I152L. Anal Biochem 2008;373:239–46.

17. Chazotte B. Labeling mitochondria with Mito-Tracker dyes. Cold Spring Harb Protoc 2011;2011:pdb.prot5648–92.

18. Bergamini C, Moruzzi N, Volta F, et al. Role of mitochondrial complex I and protective effect of CoQ10 supplementation in propofol induced cytotoxicity. J Bioenerg Biomembr 2016;48:413–23.

19. Bonora E, Evangelisti C, Bonichon F, et al. Novel germline variants identified in the inner mitochondrial membrane transporter TIMM44 and their role in predisposition to oncocytic thyroid carcinomas. Br J Cancer 2006;95:1529–36.

20. Kim SV, Mehal WZ, Dong X, et al. Modulation of cell adhesion and motility in the immune system by Myo1f. Science 2006;314:136–9.

21. Verduzco D, Amatruda JF. Analysis of cell proliferation, senescence, and cell death in zebrafish embryos. Methods Cell Biol 2011;101:19–38.

22. Mendieta-Serrano MA, Schnabel D, Lomelí H, et al. Cell proliferation patterns in early zebrafish development. Anat Rec (Hoboken) 2013;296:759–73.

23. Luo N, Li H, Xiang B, et al. Syndecan-4 modulates the proliferation of neural cells and the formation of CaP axons during zebrafish embryonic neurogenesis. Sci Rep 2016;6:25300

24. Smiley ST, Reers M, Mottola-Hartshorn C, et al. Intracellular heterogeneity in mitochondrial membrane potentials revealed by a J-aggregate-forming lipophilic cation JC-1. Proc Natl Acad Sci USA 1991;88:3671–5.

25. Chazotte B. Labeling mitochondria with JC-1. Cold Spring Harb Protoc 2011;2011:pdb.prot065490

26. Yoshihara A, Hara T, Kawashima A, et al. Regulation of dual oxidase expression and H2O2 production by thyroglobulin. Thyroid 2012;22:1054–62.

27. Cavaco BM, Batista PF, Sobrinho LG, et al. Mapping a new familial thyroid epithelial neoplasia susceptibility locus to chromosome 8p23.1-p22 by high-density single-nucleotide polymorphism genome-wide linkage analysis. J Clin Endocrinol Metab 2008;93:4426–30.

28. Jazdzewski K, Murray EL, Franssila K, et al. Common SNP in pre-miR-146a decreases mature miR expression and predisposes to papillary thyroid carcinoma. Proc Natl Acad Sci USA 2008;105:7269–74.

29. Gudmundsson J, Sulem P, Gudbjartsson DF, et al. Common variants on 9q22.33 and 14q13.3 predispose to thyroid cancer in European populations. Nat Genet 2009;41:460–4.

Cancer Genetics and Epigenetics

30. Bonora E, Rizzato C, Diquigiovanni C, et al. The FOXE1 locus is a major genetic determinant for familial nonmedullary thyroid carcinoma. *Int J Cancer* 2014;134:2098–107.

31. Bonora E, Porcelli AM, Gasparre G, et al. Defective oxidative phosphorylation in thyroid oncocytic carcinoma is associated with pathogenic mitochondrial DNA mutations affecting complexes I and III. *Cancer Res* 2006;66:6087–96.

32. Gasparre G, Porcelli AM, Bonora E, et al. Disruptive mitochondrial DNA mutations in complex I subunits are markers of oncocytic phenotype in thyroid tumors. *Proc Natl Acad Sci USA* 2007;104:9001–6.

33. Porcelli AM, Ghelli A, Ceccarelli C, et al. The genetic and metabolic signature of oncocytic transformation implicates HIF1alpha destabilization. *Hum Mol Genet* 2010;19:1019–32.

34. Bauer G. Targeting extracellular ROS signaling of tumor cells. *Anticancer Res* 2014;34:1467–82.

35. Laurent E, McCoy JW, Macina RA, et al. Nox1 is over-expressed in human colon cancers and correlates with activating mutations in K-Ras. *Int J Cancer* 2008;123:100–7.

36. Carvalho DP, Dupuy C. Role of the NADPH oxidases DUOX and NOX4 in thyroid oxidative stress. *Eur Thyroid J* 2013;2:160–7.

37. Iqbal S, Hood DA. Oxidative stress-induced mitochondrial fragmentation and movement in skeletal muscle myoblasts. *Am J Physiol Cell Physiol* 2014;306:C1176–83.

38. Li S, Xu S, Roelofs BA, et al. Transient assembly of F-actin on the outer mitochondrial membrane contributes to mitochondrial fission. *J Cell Biol* 2015;208:109–23.

39. Seri M, Cusano R, Gangarossa S, et al. Mutations in MYH9 result in the May-Hegglin anomaly, and Fechtner and Sebastian syndromes. The May-Hegglin/Fechtner Syndrome Consortium. *Nat Genet* 2000;26:103–5.

40. Seri M, Pecci A, Di Bari F, et al. MYH9-related disease: May-Hegglin anomaly, Sebastian syndrome, Fechtner syndrome, and Epstein syndrome are not distinct entities but represent a variable expression of a single illness. *Medicine (Baltimore)* 2003;82:203–15.

41. Inoue-Yamauchi A, Oda H. Depletion of mitochondrial fission factor DRP1 causes increased apoptosis in human colon cancer cells. *Biochem Biophys Res Commun* 2012;421:81–5.

42. Zhao J, Zhang J, Yu M, et al. Mitochondrial dynamics regulates migration and invasion of breast cancer cells. *Oncogene* 2013;32:4814–24.

43. Ferreira-da-Silva A, Valacca C, Rios E, et al. Mitochondrial dynamics protein Drp1 is overexpressed in oncocytic thyroid tumors and regulates cancer cell migration. *PLoS One* 2015;10:e0122308

44. Kashatus JA, Nascimento A, Myers LJ, et al. Erk2 phosphorylation of Drp1 promotes mitochondrial fission and MAPK driven tumor growth. *Mol Cell* 2015;57:537–51.

45. Pyakurel A, Savoia C, Hess D, et al. Extracellular regulated kinase phosphorylates mitofusin 1 to control mitochondrial morphology and apoptosis. *Mol Cell* 2015;58:244–54.

46. Wang Y, He H, Li W, et al. MYH9 binds to lncRNA gene PTCSC2 and regulates FOXE1 in the 9q22 thyroid cancer risk locus. *Proc Natl Acad Sci USA* 2017;114:474–9.

Cancer Genetics and Epigenetics